Biochemical and Biophysical Research Communications 822 (2026) 153918

Contents lists available at ScienceDirect

Biochemical and Biophysical Research Communications

journal homepage: www.elsevier.com/locate/ybbrc

# A click-compatible BmTyr platform for biotin-free proximity labeling and subcellular proteome profiling in primary T cells

Xin-Nan Zheng [a], Jing-Min Zeng [a], Han-Ying Huang [a], Chuang Zhao [a], Sheng-Suo Ma [a], Lin Feng [a], Hao Zhu [b], Lin Tian [a,*]

[a] State Key Laboratory of Oncology in South China, Guangdong Provincial Clinical Research Center for Cancer, Sun Yat-sen University Cancer Center, Guangzhou, 510060, PR China

[b] SANKEN, The University of Osaka, 8-1 Mihogaoka, Ibaraki-shi, Osaka, 567-0047, Japan

A B S T R A C T

Proximity labeling has revolutionized the study of dynamic subcellular proteomes by enabling the capture of transient protein interactions within living cells, yet the application of existing platforms to hard-to-transfect primary cells remains challenging. Here, we leverage a bioorthogonal proximity labeling platform based on the copper-dependent tyrosinase BmTyr to profile subcellular proteomes in primary T cells. This system catalyzes the subcellular incorporation of an alkyne-phenol probe, enabling subsequent click-compatible conjugation to versatile azide-bearing tags for fluorescence imaging and affinity enrichment for mass spectrometry. To expand the proximity labeling toolkit, we developed a custom azide-HiBiT/His tag mixture, which enables direct, antibody-independent validation using the same alkyne-phenol labeling chemistry, coupled with efficient elution and ultrasensitive chemiluminescent detection for low-input samples. Applying this platform to primary T cells not only validated known nuclear components of the TNFα signaling pathway but also revealed a previously unappreciated chromatin-associated localization for NKAP, providing new mechanistic insight beyond its previously described nuclear translocation. Collectively, our work establishes a powerful and flexible tool for sensitive, context-specific proteomic mapping in challenging physiological systems.

## 1. Introduction

In the post-genome era, the central challenge has shifted from sequencing DNA to understanding biological complexity at epigenome and proteome levels [1,2]. This includes elucidating how dynamic proteomic networks, governed by protein-protein interactions (PPIs), enable cells to respond to environmental stimuli and maintain homeostasis. A primary focus of proteomics is to map the subcellular proteome under varying conditions, identify context-specific PPIs, and characterize post-translational modifications that regulate these interactions [3,4].

Several cytological methods exist to study PPIs, such as yeast two-hybrid assays [5] and proximity ligation assays (PLA) [6]. However, these methods required the already identification of bait protein and prey protein, therefore representing more as the confirmation instead of exploration. The co-immunoprecipitation (co-IP) and subsequent mass spectrometry (MS) analysis remain the gold standard for systemically direct biochemical identification of PPIs [7,8]. However, this pipeline has significant limitations: it often requires extensive optimization, as harsh lysis conditions can disrupt weak or transient interactions [9]. Furthermore, cell lysis can create artificial microenvironments, allowing bait proteins to interact with prey proteins they do not normally encounter *in vivo*, leading to potential false-positive results [10].

To overcome these inherent limitations of traditional co-IP, proximity-dependent protein labeling platforms have been developed. These platforms can be categorized based on their enzymatic mechanisms, including engineered biotin ligases [11–14], the NEDDylator system (which hijacks the endogenous NEDDylation pathway) [15], Pup ligases [16], and enzymes that oxidize phenol to react with nucleophilic residues of proximal proteins [17]. The most established of these, BioID, utilizes a promiscuous mutant of the *E. coli* biotin ligase BirA to indiscriminately biotinylate proximal proteins [18]. Its enhanced version, TurboID, offers improved catalytic kinetics [13,19]. A significant drawback of biotin ligase-based systems, however, is the high background signal caused by endogenous biotinylation processes (e.g., in carboxylase reactions during metabolism) [20]. This lack of bioorthogonality is also a concern for the NEDDylator system [15].

To circumvent background from endogenous pathways, the Pup ligase system was developed to conjugate a Pup(E) peptide tag to lysine residues [16]. However, this method requires substantial genetic engineering as the Pup(E) peptide is not cell-permeant and must be expressed intracellularly. In contrast, phenol probe-based proximity

* Corresponding author.
*E-mail address:* tianlin@sysucc.org.cn (L. Tian).

https://doi.org/10.1016/j.bbrc.2026.153918
Received 7 May 2026; Accepted 8 May 2026
Available online 12 May 2026

labeling employs small, cell-permeant phenol probes that can be functionalized with handles like biotin or alkyne groups, offering greater experimental flexibility [21].

The oxidization of phenol has also been used to modify the amino acids of proximity proteins. This oxidization can occur via two primary enzymatic routes: peroxidases, which convert phenol into short-lived phenoxyl radicals [22], and tyrosinases, which oxidize phenol to *o*-quinone [23]. While peroxidase-based systems exhibit extremely fast kinetics, making them ideal for capturing transient interactions [24], their dependence on hydrogen peroxide ($H_2O_2$) may poses cytotoxic risks [25]. Although $H_2O_2$ can be rapidly aspirated and quenched within seconds for adherent cultured cells, suspension cells require centrifugation during the labeling reaction, which prolongs exposure to $H_2O_2$-containing buffers and increases cytotoxicity. In contrast, tyrosinase-based systems, such as BmTyr [26,27], provide a milder labeling alternative and therefore represent an alternative approach, including proteome profiling in primary cultured cells and even *in vivo* applications.

Here, we harness the BmTyr tyrosinase system to profile the subnuclear proteome in primary cultured T cells, using a cell-permeant alkyne-phenol probe [28]. This strategy incorporates a bio-orthogonal alkyne handle into proximal proteins, enabling their conjugation via click chemistry to diverse azide-linked reagents for downstream applications such as fluorescence imaging and MS. To facilitate validation of MS hits, we developed a custom dual azide-tag system (HiBiT/His). This system enables highly sensitive chemiluminescent detection and efficient elution for downstream Western blot analysis in an antibody-independent manner. Application of this method to T cells not only validated known components of the TNFα signaling pathway but also highlighted a histone-associated localization for NKAP. Collectively, our work establishes a powerful and versatile proximity labeling tool for sensitive and context-specific proteomic mapping in physiologically relevant and challenging systems.

## 2. Results

### 2.1. Comparison of biotin-phenol and alkyne-phenol for BmTyr proximity labeling

To enable subcellular proteome labeling, we expressed two distinct BmTyr constructs via mRNA transfection in NIH3T3 cells: a Flag-tagged BmTyr (Flag-BmTyr) and a nuclear-localized, mCherry- and H2B-tagged BmTyr (mCherry-BmTyr-H2B). This strategy allowed us to confirm the subcellular localization of the enzyme and its correspondingly labeled proteins. Using the previously established probe biotin-phenol, we observed that Flag-BmTyr and its proximity-labeled proteins were distributed ubiquitously throughout the cell, whereas mCherry-BmTyr-H2B and its labeled proteome were restricted to the nucleus, validating the expected localization of each construct (Fig. S1).

In addition to subcellular protein labeling, we also engineered a fusion between BmTyr and Zfp683, a zinc-finger nuclear protein specifically expressed in memory T cells and NK-like T cells [29]. We constructed both N-terminal BmTyr fusion (BmTyr-Zfp683-V5) and C-terminal BmTyr fusion (Zfp683-BmTyr-Flag). Immunofluorescence imaging revealed that the N-terminal BmTyr fusion retained nuclear-restricted localization comparable to that of V5-tagged Zfp683 alone, albeit with a modest reduction in expression level (Fig. S2A and B). In contrast, the C-terminal BmTyr fusion exhibited diffuse localization and failed to concentrate in the nucleus (Fig. S2C), suggesting that fusion to the C-terminus of Zfp683 disrupts elements critical for its nuclear import or stability. Notably, the labeling pattern of Zfp683-V5 predominantly localized with DAPI-dense regions, indicative of heterochromatin enrichment. This observation aligns with previously reported evidence that Zfp683 functions as a transcriptional repressor [30].

We next evaluated an alkyne-phenol probe as a potential alternative. Compared with biotin-phenol, alkyne-phenol possesses a smaller molecular weight (Fig. 1A) and offers practical advantages in terms of lower working concentration and improved signal-to-noise ratio in our experimental system (Fig. 1B and C). To optimize labeling specificity, we titrated the alkyne-phenol concentration. While concentrations below 0.015 mM yielded no detectable signal, 0.5 mM resulted in diffuse and non-nuclear labeling, indicative of non-specific probe binding. An intermediate concentration of 0.15 mM alkyne phenol provided optimal signal-to-background with precise nuclear restriction (Fig. 1D and E). This optimized condition was subsequently used for all downstream applications, including MS analysis and immunoprecipitation for Western blotting.

### 2.2. Efficient elution of alkyne-labeled proteins using a custom dual-tag system

Beyond fluorescence imaging, we aimed to develop a robust method for the affinity purification of the proximity-labeled proteome. While azide-biotin is the most common reagent for CuAAC-mediated enrichment and subsequent MS, the exceptionally high affinity between biotin and streptavidin makes it difficult to elute the labeled proteome for direct validation of MS hits [31].

Therefore, we defined the ideal enrichment tag as needing to be (1) highly sensitive, (2) bioorthogonal, and (3) efficiently elutable. The HiBiT peptide tag meets the first two criteria. Its detection relies not on an antibody, but on complementation with the LgBiT protein to form an active Nano luciferase, enabling highly sensitive chemiluminescent detection in the presence of furimazine [32,33]. Moreover, it can theoretically be eluted from its cognate anti-HiBiT antibody beads [34].

Accordingly, we synthesized a custom azide-HiBiT tag for conjugation to the alkyne-labeled proteome (Fig. 2A). While the tag itself was successfully conjugated with minimal protein loss during click reaction (Fig. S3A and B) and detected and excess free tag was efficiently removed by dialysis (Fig. S3C), affinity purification using anti-HiBiT magnetic beads was unsuccessful, with most tagged proteins appearing in the flow-through (Fig. S3D). We hypothesized that this failure resulted from either an insufficient local protein concentration at the beads or a steric constraint due to a suboptimal linker length between the azide and the HiBiT peptide. Attempts to mitigate the concentration issue by adding inert carrier protein bovine serum albumin (BSA) did not improve recovery (Fig. S3E).

Given the low enrichment efficiency and high cost of the anti-HiBiT beads, we devised an alternative strategy. We reasoned that mixing the azide-HiBiT tag with a conventional azide-polyhistidine (His) tag would enable efficient elution via Ni-NTA magnetic beads, while retaining the ultrasensitive HiBiT-based detection [35]. We therefore combined our custom azide-HiBiT tag with commercially available azide-6 × His or azide-10 × His tags at an equimolar ratio (Fig. 2B and C). This dual-tag system proved highly effective. Both His-tag variants successfully enriched the alkyne-labeled proteome, with azide-10 × His providing slightly superior enrichment efficiency (Fig. 2D and E). The HiBiT tag subsequently enabled sensitive chemiluminescent detection of the eluted proteins, fulfilling all three design criteria.

To further demonstrate the elution efficiency of our dual-tag system, we performed a side-by-side comparison with the conventional biotin–streptavidin enrichment. Under harsh elution conditions (high concentration of biotin or formamide at 95 °C), only a small fraction of biotinylated proteins was released from streptavidin beads, with the majority remaining bead-bound as revealed by subsequent SDS boiling. In contrast, our dual-tag system enabled efficient elution under mild conditions, with substantially less protein remaining on the beads after elution (Fig. 2F). These results underscore the practical advantage of our system for validation workflows requiring recovery of intact proteins.

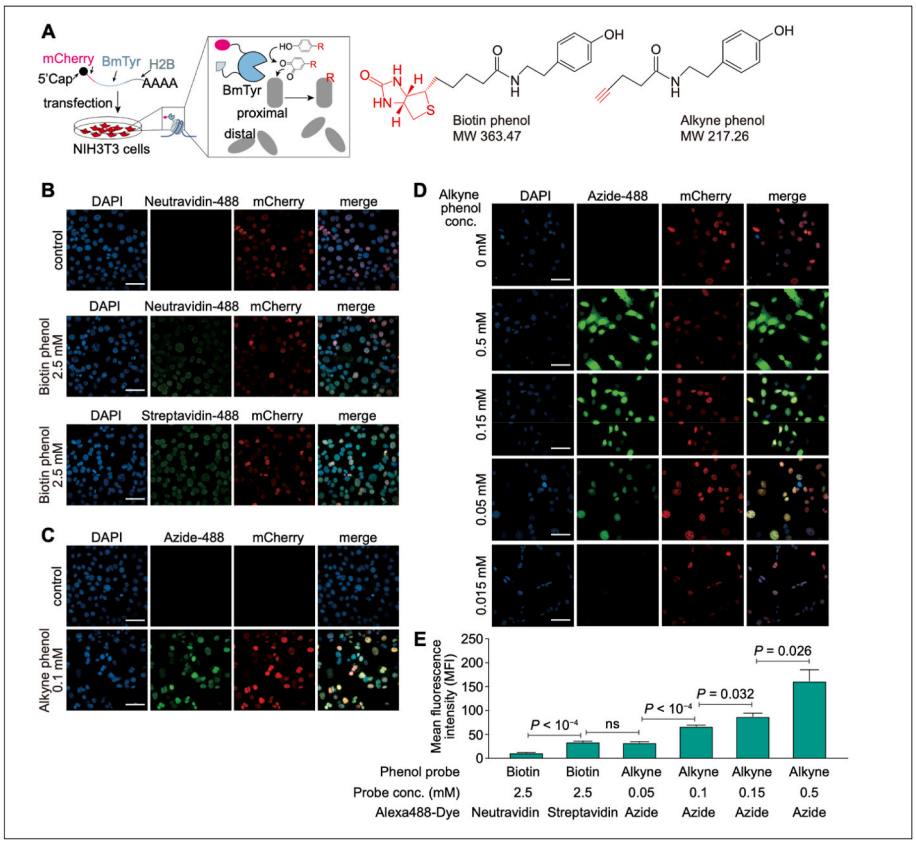


**Fig. 1.** Comparison of biotin-phenol and alkyne-phenol probes for BmTyr-mediated proximity labeling **A)** Schematic of mRNA-based expression for BmTyr-fusion proteins and the chemical structures of the biotin-phenol and alkyne-phenol probes, with their respective molecular weights indicated. **B,C)** Immunofluorescence imaging of the nuclear-localized BmTyr-H2B fusion protein (red) and its proximity-labeled proteome (green) in NIH3T3 cells. Labeling was performed using either the (**B**) biotin-phenol probe (detected with Alexa Fluor 488-conjugated neutravidin/streptavidin) or the (**C**) alkyne-phenol probe (conjugated via CuAAC to Alexa Fluor 488-azide) (scale bars, 50 μm). **D)** Optimization of the alkyne-phenol probe concentration. Representative immunofluorescence images at indicated probe concentrations (BmTyr-H2B in red, labeled proteome in green) (Scale bar, 50 μm). **E)** Quantification of the labeled proteome mean fluorescence intensity for each condition. Data are presented as mean ± s.e. *P* value was calculated by two-tailed paired Student's *t*-test. (For interpretation of the references to colour in this figure legend, the reader is referred to the Web version of this article.)

### *2.3. BmTyr for nuclear proteome profiling in primary T cells via mass spectrometry*

Having established and optimized the BmTyr platform in NIH3T3 cells, we next sought to apply it to the more physiologically relevant but technically challenging system of primary cultured T cells. This transition required addressing two major hurdles: (1) confirming the biosafety of copper ($Cu^{2+}$) supplementation in primary cells, and (2) achieving efficient protein expression within the limited *in vitro* lifespan of primary T cells.

To directly assess $Cu^{2+}$ cytotoxicity, we incubated T cells with a range of $CuCl_2$ concentrations (10 μM to 1000 μM). Cell viability was quantified using a dual-staining flow cytometry assay: cells were pre-labeled with the live/dead dye NucFixRed (which covalently binds nuclei of apoptotic/dead cells) [36], followed by DAPI staining after $Cu^{2+}$ incubation. Cells that were DAPI-positive but NucFixRed-negative represented newly induced cell death attributable to $Cu^{2+}$. This assay confirmed that our working concentration of 10 μM $Cu^{2+}$ induced minimal toxicity, with a significant increase in cell death becoming apparent only at concentrations exceeding 30 μM (Fig. 3A).

To maximize efficiency within the constrained cultivation window, we employed a nanoparticle-mediated mRNA transfection strategy [37]. This approach enabled rapid expression of the BmTyr-fusion protein within 12 h (Fig. 3B) and offered the critical advantage of low immunogenicity, avoiding the confounding innate immune activation triggered by cytosolic DNA [38]. Transfection efficiency, assessed by flow cytometry, exceeded 50%, confirming robust delivery in these hard-to-transfect cells (Fig. 3C).

We then applied this optimized system to profile changes in the nuclear proteome of T cells upon stimulation with tumor necrosis factor-alpha (TNFα), a key cytokine in T cell biology known to induce rapid nuclear translocation of factors like NF-κB [39,40]. This pathway served as an ideal proof-of-concept for our proximity labeling platform. We engineered wild-type (*WT*) and TNFR1 knockout ($TNFR1^{KO}$) T cells to express the nuclear-localized mCherry-BmTyr-H2B fusion protein, treated them with TNFα (10 ng $ml^{-1}$, 6 h), and performed proximity labeling.

Following labeling with the alkyne-phenol probe, labeled proteins were conjugated to azide-functionalized magnetic beads via click chemistry, enabling stringent washes to reduce background. After on-bead digestion, the resulting peptides were analyzed by MS. The MS quality metrics indicated typical peptide lengths (7-26 amino acids) and coverage (Fig. S4). For the on-bead digestion MS samples, we successfully identified over 6000 peptides mapping to more than 1600 proteins (Fig. S4A–D). In comparison, global input MS samples yielded approximately 68,000 peptides mapping to more than 7000 proteins, with comparable depth and intensity across all experimental conditions (Fig. S4E–H).

As anticipated, TNFα treatment triggered the nuclear enrichment of proteins involved in Toll-like receptor signaling and I-κB phosphorylation, hallmarks of NF-κB pathway activation (Fig. 3D) [40,41]. Notably, this response was profoundly attenuated in $TNFR1^{KO}$ T cells, validating

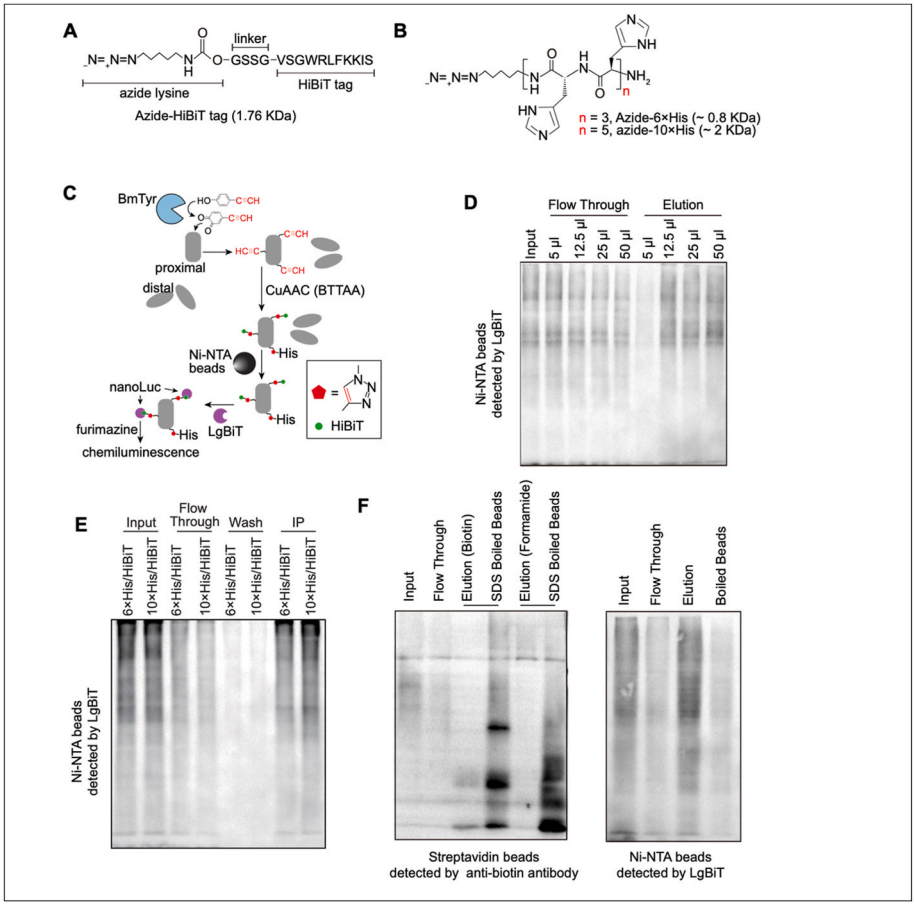


**Fig. 2.** Immunoprecipitation and chemiluminescent detection of the proximity-labeled proteome using a dual azide-tag system **A,B**) Chemical structures of the custom-synthesized enrichment tags: (**A**) azide-HiBiT tag and (**B**) azide-polyhistidine tag (6 × His and 10 × His variants), with their respective molecular weights indicated. **C**) Schematic workflow for the enrichment and detection of alkyne-labeled proteins. Proximity-labeled proteins are conjugated via CuAAC to an equimolar mixture of azide-HiBiT and azide-His tags, followed by enrichment using Ni-NTA magnetic beads and subsequent chemiluminescent detection via HiBiT/LgBiT complementation with the furimazine substrate. **D**) Titration of Ni-NTA bead volumes to optimize enrichment of HiBiT/His tag-conjugated proximity-labeled proteins. **E**) Western blot analysis validating the dual-tag enrichment strategy. Proximity-labeled proteins from cells expressing BmTyr-H2B were conjugated with either azide-6 × His or azide-10 × His (mixed with azide-HiBiT), enriched on Ni-NTA beads, eluted, and detected based on LgBiT complementation. Comparison shows efficient enrichment with both tags, with azide-10 × His exhibiting marginally superior performance. **F**) Side-by-side comparison of elution efficiency between the biotin–streptavidin system and the HiBiT/His-tag system (Ni-NTA based). The dual-tag system enabled efficient elution under mild conditions, whereas biotinylated proteins remained largely bead-bound even under harsh elution conditions.

the specificity of our assay (Fig. 3D).

Based on the proximity labeling MS analysis, we identified 116 nuclear proteins whose abundance changed upon TNFα treatment according to the following fold-change enrichment criteria: (1) proteins with a fold change >1.5 were considered enriched, and (2) proteins with a fold change <1/1.5 (i.e., <0.67) were considered decreased. Importantly, the abundance of these 116 nuclear proteins was largely unchanged in the global proteome input controls, indicating that the observed changes are specific to the nuclear compartment (Fig. 3E). Unbiased clustering of 116 differentially enriched nuclear proteins revealed a subset of 20 proteins specifically enriched in TNFα-treated *WT* cells but absent in *TNFR1*$^{KO}$ cells under the same condition (Fig. 3F). Gene ontology analysis of this subset highlighted significant overrepresentation of terms related to transcriptional and epigenetic regulation (Fig. 3G), consistent with the chromatin-focused design of our H2B-BmTyr construct and implicating TNFα/TNFR1 signaling in modulating the nuclear protein landscape [42].

### 2.4. Validation of primary T cell proteomic data using the azide-HiBiT/His mixed tag

From our proteomic screen, NF-κB Activating Protein (NKAP) was selected for proof-of-concept validation given its established role downstream of NF-κB signaling (Fig. 4A) [43]. Although biochemical subcellular fractionation revealed that the majority of NKAP protein remained in the cytoplasmic fraction even after TNFα stimulation (Fig. 4B), we applied our azide-HiBiT/His mixed-tag immunoprecipitation platform to primary T cells from *WT* or *TNFR1*$^{KO}$ backgrounds, with or without TNFα stimulation. Cells expressing similar levels of the nuclear-localized mCherry-BmTyr-H2B fusion protein were labeled with the alkyne-phenol probe (Fig. 4C). While total NKAP levels and overall labeling efficiency were comparable across conditions, His-tag enrichment followed by HiBiT-based chemiluminescent detection revealed a significant enrichment of NKAP in TNFα-stimulated *WT* T cells (Fig. 4D). Our results suggest that while TNFα-TNFR1 signaling does not alter total nuclear NKAP levels, it enhances the chromatin-associated fraction of NKAP, as captured by our H2B-BmTyr proximity labeling system. This finding directly validates the results obtained from MS and indicates that TNFR1-mediated signaling promotes the stable association of NKAP with chromatin, consistent with prior reports implicating NKAP in chromatin remodeling via histone deacetylase (HDAC) complexes [44,45].

To demonstrate the generalizability and robustness of our platform, we have now applied it to an additional primary cell type: bone marrow-

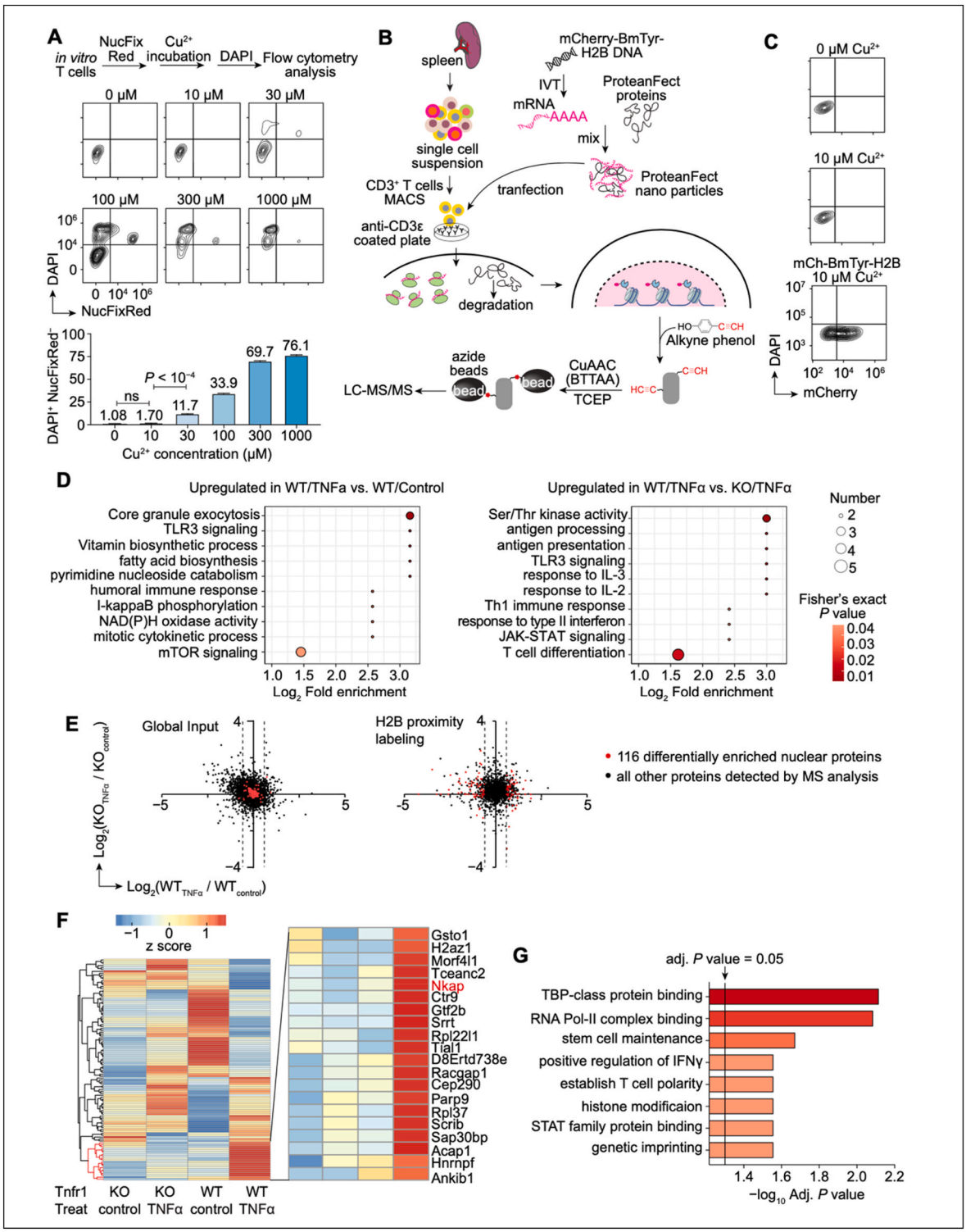


**Fig. 3.** Proximity labeling and mass spectrometry analysis of the nuclear proteome in primary T cells **A**) Assessment of $Cu^{2+}$ cytotoxicity in primary T cells. Cells were treated with indicated concentrations of $CuCl_2$, and viability was quantified via flow cytometry. Data are presented as mean ± s.e.m. *P* value was calculated by two-tailed paired Student's *t*-test. **B**) Schematic overview of the experimental workflow: nanoparticle-mediated mRNA delivery of mCherry-BmTyr-H2B, proximity labeling with alkyne-phenol, conjugation to azide-magnetic beads via CuAAC, and on-bead digestion for mass spectrometry analysis. **C**) Flow cytometry analysis confirming low cytotoxicity at 10 μM $Cu^{2+}$ and high transfection efficiency of mCherry-BmTyr-H2B mRNA in primary T cells. **D**) Gene ontology (GO) enrichment analysis of nuclear proteins significantly altered upon (**D**) TNFα stimulation (left) or TNFR1 knockout (right). **E**) Dot plots showing the protein abundance changes of 116 nuclear proteins in global MS input samples (left) versus H2B-proximity-labeled on-bead digestion MS samples (right). The x-axis represents the $Log_2$ fold change in *WT* T cells (TNFα-treated versus untreated), and the y-axis represents the $Log_2$ fold change in $TNFR1^{KO}$ T cells (TNFα-treated versus untreated). **F**) Heatmap of hierarchical clustering based on the abundance of 116 differentially enriched nuclear proteins across the four experimental groups: $Tnfr1^{KO}$ (untreated), $Tnfr1^{KO}$ + TNFα, *WT* (untreated), and *WT* + TNFα. **G**) Over-representation analysis of the 20 nuclear proteins specifically enriched in TNFα-treated *WT* T cells, highlighting biological processes related to transcriptional and chromatin regulation.

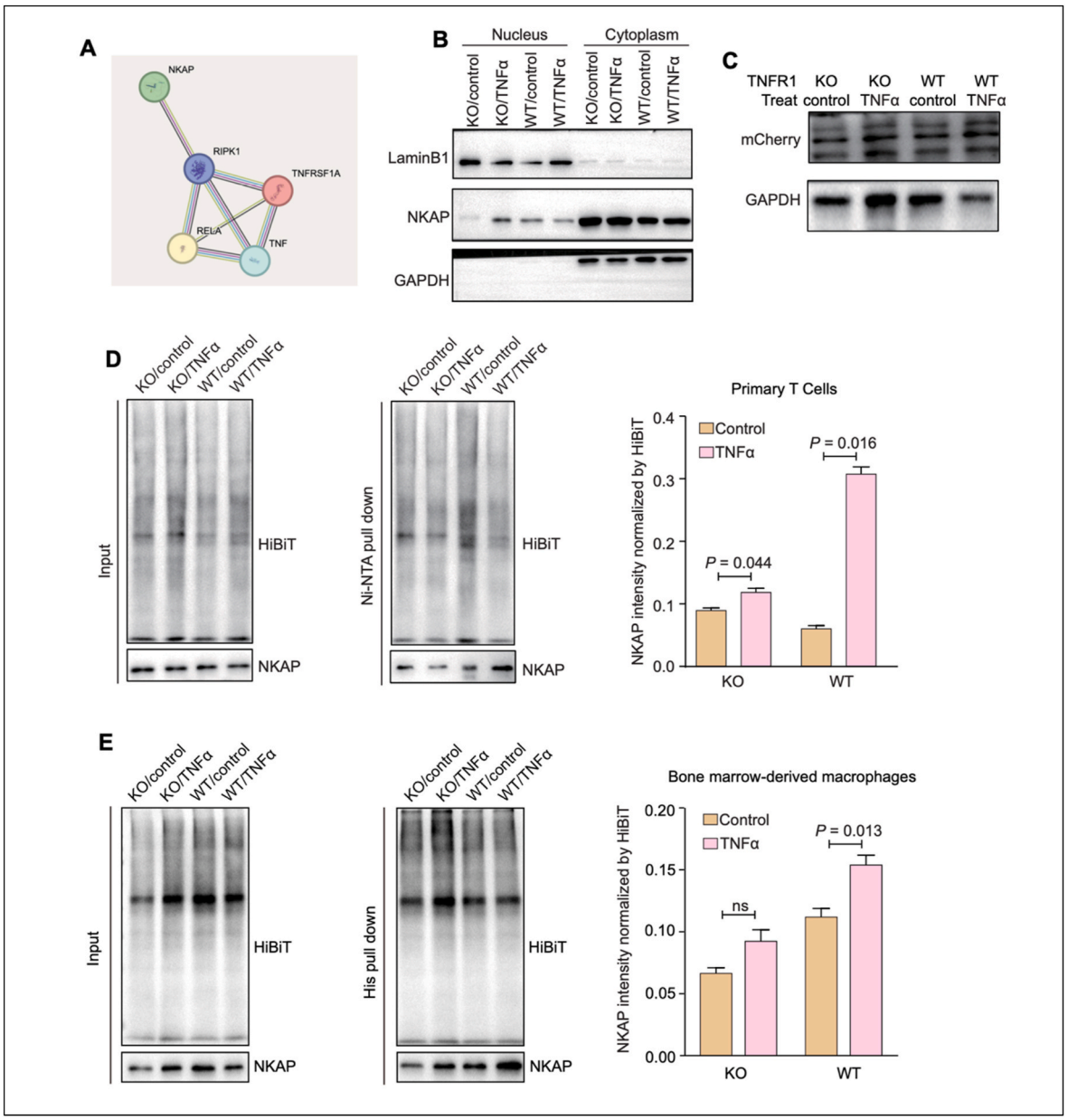


**Fig. 4.** Validation of NKAP as a chromatin-associated downstream effector of TNFα signaling **A**) Protein interaction network of TNFα signaling components, including NKAP, generated using the STRING database. **B**) Subcellular fractionation and Western blot analysis of NKAP distribution in the nucleus and cytoplasm across the four experimental groups: *KO* (control), *KO* + TNFα, *WT* (control), and *WT* + TNFα. **C**) Western blot analysis confirming comparable expression levels of the mCherry-BmTyr-H2B fusion protein across all experimental groups. **D, E**) Validation of NKAP enrichment using the dual azide-HiBiT/His tag system in primary T cells (**D**) and bone marrow-derived macrophages (BMDMs) (**E**). (Left) HiBiT-based chemiluminescence detection confirms comparable proximity labeling efficiency across samples. Whole-cell lysate Western blot shows similar total NKAP expression. (Right) Following Ni-NTA enrichment of His-tagged proteins, HiBiT signal quantification reveals specific enrichment of NKAP only in TNFα-stimulated *WT* T cells. HiBiT intensity was used for normalization. *P* value was calculated by two-tailed paired Student's *t*-test.

derived macrophages (BMDMs), a cell type distinct from T cells that also responds to TNFα stimulation. Consistent with our findings in T cells, TNFα treatment led to a specific enrichment of NKAP in wild-type BMDMs, but not in TNFR1 knockout BMDMs. This result confirms that the TNFR1-dependent chromatin association of NKAP is reproducible across distinct primary cell types, thereby supporting the generalizability of our platform (Fig. 4E).

Collectively, these data achieve two objectives. First, we provide experimental validation of a key proteomic hit using our novel dual-tag detection platform. Second, we demonstrate a previously unappreciated histone-associated localization of NKAP, suggesting that TNFα–TNFR1 signaling enhances the association of NKAP with chromatin, a phenomenon that extends beyond T cells.

## 3. Discussion

In this study, we applied a BmTyr-based proximity labeling platform for subcellular proteome mapping in primary T cells. The system employs a small, cell-permeant alkyne-phenol probe, whose incorporated alkyne handle serves as a bio-orthogonal anchor for downstream conjugation via click chemistry. To maximize the utility of this platform, we linked the labeled proteome to a suite of azide-conjugated reagents, including dyes for imaging and beads for enrichment. A key modification is the development of a custom dual azide-tag system (HiBiT/His),

designed to overcome two major bottlenecks in validating mass spectrometry (MS) data: the inefficient elution common in streptavidin-based methods and the need for reliable signal normalization. Using this integrated approach, we not only profiled the nuclear proteome but also gained novel biological insight. Specifically, we discovered that the regulatory protein NKAP exhibits enhanced association with histone proteins upon TNFα stimulation, a finding that refines the existing model of its activation from one of simple nuclear translocation to one of specific chromatin engagement.

A primary consideration for the BmTyr system is the potential cytotoxicity associated with copper ($Cu^{2+}$) supplementation during labeling. In our experiments, however, flow cytometry analysis revealed no significant increase in cell death at the working concentration of 10 μM $CuCl_2$. Notably, this concentration is 400 times lower than that typically required for copper-catalyzed azide-alkyne cycloaddition (CuAAC, ~4 mM), underscoring a favorable toxicity profile. Interestingly, we observed a discrepancy between different cell viability assays. While the CCK-8 assay aligned with our flow cytometry data in indicating low toxicity [26], the MTS assay showed markedly higher cytotoxicity at 10 μM $CuCl_2$ [27]. This divergence likely stems from the well-documented interference of $Cu^{2+}$ with the mitochondrial dehydrogenase activity measured in the MTS assay [46], suggesting it may overestimate copper-induced cytotoxicity in this context. An intriguing potential strategy to further mitigate any residual copper exposure is to preassembled $Cu^{2+}$-BmTyr complex prior to its introduction to the cellular environment [26]. This approach, however, is constrained by the poor cell permeability of the pre-assembled complex, limiting its current applicability to the labeling of extracellular or cell-surface proteins.

Another consideration for tyrosinase-based proximity labeling (e.g., BmTyr) is its relatively large labeling radius (up to 1 μm) and labeling time (~10 min) compared to peroxidase-based systems (e.g., APEX2, labeling radius ~20 nm, labeling time ~1 min) [22,47–49]. To overcome the spatial and temporal resolution limitations imposed by diffusion-controlled chemical activation and quenching, photocatalytic proximity labeling platforms offer a promising alternative to enzyme-based strategies (labeling radius 2–100 nm, labeling time <1 min) [50]. These platforms employ catalytic photosensitizers that generate reactive species locally upon light exposure, enabling covalent modification of proximal biomolecules with high spatiotemporal precision.

A critical methodological aspect of this study is our use of mRNA transfection, rather than plasmid or viral vectors, to deliver the BmTyr-fusion construct into primary T cells. This strategy is pivotal for several reasons. First, it circumvents the robust innate immune activation triggered by cytosolic double-stranded DNA [51,52], a common artifact of plasmid transfection or viral infection that could confound downstream signaling analysis in immune cells. Second, mRNA enables rapid and transient protein expression (typically within 12 h), which aligns optimally with the limited *in vitro* lifespan of primary, non-immortalized cells. This efficient timeline allows for precise proximity labeling within a viable cellular window, maximizing physiological relevance while minimizing culture-induced artifacts.

Overall, this study establishes the feasibility and utility of the BmTyr-based proximity labeling platform for proteomic profiling in primary T cells. We have developed a complete experimental and analytical framework, from mRNA-mediated delivery and bio-orthogonal labeling to sensitive validation via our custom HiBiT/His tag system. We are confident that this versatile pipeline can be readily adapted to study other primary, hard-to-transfect cell types, enabling the capture of weak or transient interactions that are often lost in conventional assays. By providing a powerful tool to illuminate context-specific and dynamic proteomes in physiologically relevant systems, this work opens new avenues for mechanistic discovery in immunology and beyond.

### 3.1. Limitations of the study

Our study introduces a dual azide-His/HiBiT tag system for the efficient enrichment and sensitive detection of the alkyne-labeled proteome. A key assumption of this method is that a target protein bears at least two alkyne groups, enabling its simultaneous capture via the His tag and detection via the HiBiT tag. However, this approach may fail to recover weak or transient interactors that incorporate only a single alkyne moiety, potentially underestimating certain interactions within the labeled proteome.

Beyond this technical consideration, the biological insights generated here also point to important future directions. While our platform successfully identified the recruitment of NKAP to chromatin upon TNFα stimulation, the precise molecular mechanism of this association and its functional impact on histone modification and gene expression remain to be fully elucidated. Future studies employing targeted genetic or pharmacological perturbations of NKAP, combined with epigenomic and transcriptomic analyses, will be essential to define its role in this signaling pathway and validate its biological significance.

## 4. Methods

### 4.1. Cell culture

Human embryonic kidney 293T cells and mouse embryonic fibroblast NIH3T3 cells (gifts from P.H Zhou, Sun Yat-sen University Cancer Center) were cultured in DMEM/High Glucose medium (Thermo Fisher, #C11995500BT). Both media contained 10% FBS (Gibco, #A3160802), 100 IU $ml^{-1}$ penicillin/streptomycin, 100 μg $ml^{-1}$ amphotericin B (Lonza, #17-745E) and 200 nM L-Glutamine (Gibco, #25030081).

All cells were grown in a humidified incubator at 37 °C, with 5% $CO_2$, and were tested regularly for mycoplasma contamination (Vazyme, #D101).

### 4.2. Mouse used

All animal work was done in accordance with a protocol approved by Institutional Animal Care and Use Committee (IACUC) at the Sun Yat-sen University Cancer Center (SYSUCC), with Approval Number L025504202108022.

The *wild-type* mice (N000013) and *Tnfrsf1a knockout* ($Tnfr1^{KO/KO}$, T013927) mice (both from GemPharmatech) are in C57BL/6 background. Age-matched *Wild-type* mice and $Tnfr1^{KO/KO}$ mice (6−8 week-old) were used to isolate splenic T cells.

The room is controlled at stable temperature ~22 °C within ~50% humidity, 12-h light/12-h dark cycle (on from 7:30−19:30), 10−15 fresh air exchanges hourly.

### 4.3. Mouse primary T cell isolation and stimulation

The mice were euthanized by $CO_2$. Single-cell suspensions of splenocytes were prepared by cutting the spleen into small pieces and transferring them to a tissue digestion C-tube (Miltenyi) containing 3 ml of PBS supplemented with 2 mM EDTA. The tissues were mechanically dissociated using a Single-cell Suspension Dissociator (RWD Life Science). Specifically, the "m_Lung_2" program was run to maximize the extraction of lymphocytes, followed by a 5-min incubation at room temperature with DNase I (0.1 mg $ml^{-1}$, Sigma, #10104159001). After a second run of the "m_Lung_02" program, the digestion mixture was filtered through a 70-μm cell strainer and was then centrifuged at 500×*g* to obtain the cell pellets. Cellular debris and red blood cells were removed by the Debris Removal Solution (Miltenyi, #130-109-398) and 1 × RBC Lysis Buffer (Biolegend, #420301), respectively, as per manufacturer's instructions.

T cells were enriched by mouse CD3 MicroBeads (RWD Life Science, #K1301-10) as per manufacturer's protocol. The anti-CD3-coated 24-

well plate was prepared by an overnight incubation with 300 μl anti-CD3ε antibodies (5 μg $ml^{-1}$ in PBS; Biolegend #100302) at 4 °C. Next, $1 \times 10^6$ naive T cells were cultured in 500 μl per well of T cell culture medium (X–VIVO 15 medium (04-418Q) supplemented with 10% heat-inactivated FBS, 100 IU ml−1 penicillin/streptomycin, and 25 ng $ml^{-1}$ amphotericin B, 55 μmol $l^{-1}$ β-Mercaptoethanol, 10 ng $ml^{-1}$ IL-2 (Novoprotein, #CK24), 2 μg $ml^{-1}$ anti-CD28 antibody (Biolegend #102116)). The cells were incubated at 37 °C with 5% $CO_2$ for 2 days.

### 4.4. Bone Marrow-Derived Macrophage (BMDM) isolation, culture, and transfection

Femurs from wild-type or *TNFR1*$^{KO}$ C57BL/6J mice were flushed with PBS to collect bone marrow cells. Debris was removed (Miltenyi, #130-109-398), and red blood cells were lysed (Biolegend, #420301), as per manufacturer's protocol. A total of $6 \times 10^6$ cells were seeded in a 10-cm non-tissue culture-treated dish and cultured in BMDM medium (10% FBS, 100 IU $ml^{-1}$ penicillin/streptomycin, 100 μg $ml^{-1}$ amphotericin B (Lonza, #17-745E), supplemented with 20 ng $ml^{-1}$ M-CSF (Novoprotein, CB34)) for 6 days to allow macrophage differentiation. On day 6, BMDMs were transfected with mCherry-BmTyr-H2B mRNA. After overnight incubation, cells were treated with TNFα or vehicle control, followed by incubation with the alkyne-phenol probe to label histone-associated proteins.

### 4.5. mRNA in vitro transcription

The IVT-BmTyr-Flag and IVT-H2B-BmTyr-mCherry vectors were generated by cloning the BmTyr-Flag and H2B-BmTyr-mCherry cassettes into the *in vitro* transcription synthesis template (Genewiz). Both cassettes were amplified via PCR using Q5 High-Fidelity Master Mix (NEB, M0492S). During amplification, the forward and reverse primers were appended with NheI and BstEII cutting sites, respectively. The amplified DNA fragments and vector template were digested with NheI_HF (NEB, R3131) and BstEII_HF (NEB, R3162), and were subsequently assembled using T4 DNA ligase (NEB, M0202).

The coding sequence of Zfp683-V5 was obtained by gene synthesis. Fusion constructs, including Zfp683-BmTyr-Flag and BmTyr-Zfp683-V5, were assembled and inserted into the IVT backbone using the NEBuilder HiFi DNA Assembly Kit (NEB, E2621S).

The *in vitro* transcription synthesis plasmids (Genewiz) were linearized using the restriction enzyme BspQI (Vazyme, GMP4302-PC), with the cutting site located just downstream of the homo-polyA sequence. The linearized DNA was purified with DNA clean beads (Vazyme, N411) and used as the template for the *in vitro* transcription synthesis mixture (SynthGene, C3111), allowing for the simultaneous capping of mRNA. Particularly, UTP was replaced by the chemically modified N1–MepUTP to reduce the immunogenicity of transcribed mRNA. The mixture was incubated at 37 °C for 2 h, after which DNase I (0.04 U $\mu l^{-1}$, SynthGene, 10211) was added and incubated for additional 10 min to digest the DNA template. The *in vitro* synthesized mRNA was purified using RNA clean beads (Vazyme, N412). The eluted mRNA was diluted to 1 μg $\mu l^{-1}$ and stored at −80 °C.

### 4.6. Cell transfection

Before the transfection of NIH3T3 cells, the cultured medium was replaced with pre-warmed, antibiotic-free competent medium. For a 24-well plate, 0.5 μg of mRNA in 10 μl of Opti-MEM medium was mixed with 1 μl of GoldenTran-mRNA (Golden Transfer Technology, 220521005) in an additional 10 μl of Opti-MEM medium. This mixture was incubated at room temperature for 10 min before being added dropwise to the well.

The transfection of stimulated mouse T cells was performed using ProteanFect Transfection Reagent (Nanoportal Biotech) according to the manufacturer's instructions. In brief, $1 \times 10^6$ to $1.5 \times 10^6$ stimulated T cells in a 24-well plate were washed with pre-warmed Opti-MEM medium to remove FBS and then resuspended in pre-warmed Opti-MEM medium. Concurrently, the transfection mixture for 24-well cells was prepared as follows: 2.5 μg of mRNA, 3.5 μl of Reagent B, and 50 μl of Reagent C were added to 200 μl of Reagent A. The suspended T cells were combined with the transfection mixture and transferred to a 24-well plate, followed by incubation at 37 °C for 20 min. The cells were washed once with culture medium and then incubated at 37 °C with 5% $CO_2$ for 12 to 16 h for $Cu^{2+}$ loading.

### 4.7. $Cu^{2+}$ loading for BmTyr and probe incubation

The culture medium was removed, and the cells expressing BmTyr-conjugated proteins were washed once with pre-warmed HBSS+ (HBSS (Biosharp, BL559A) with 20 mM HEPES (HyClone, SH30237.01), 2 mM $CaCl_2$ (Aladdin, C110769), and 1.2 mM $MgSO_4$ (Aladdin, M475695)). Subsequently, the cells were incubated in HBSS + containing 10 μM $CuCl_2$ (Aladdin, C106775) at 37 °C with 5% $CO_2$ for 1 h to facilitate the binding of $Cu^{2+}$ to BmTyr.

After the loading of $Cu^{2+}$, the HBSS + medium was replaced with pre-warmed competent medium containing phenol probes (Biotin phenol, 2.5 mM (TargetMol, T19209); Alkyne phenol, 0.15 mM (MCE, HY-131442)) and incubated at 37 °C for an additional 10 min for proximity labeling of proteins. Following probe labeling, the cells were washed twice with ice-cold PBS to prepare for downstream analyses, including immunostaining, flow cytometry, or protein detection.

### 4.8. Immunostaining and flow cytometry

Immunocytofluorescence staining of NIH3T3 cells were performed using Millicell EZ SLIDE (Millipore, PEZGS0816). The cells were fixed with freshly diluted 4% paraformaldehyde (PFA) for 20 min at room temperature and subsequently washed three times with PBS. Blocking was performed using a Blocking Buffer, composed of 1% BSA (Jackson ImmunoResearch, 001-000-162), 10% normal donkey serum (Jackson ImmunoResearch, 017-000-121) and 0.25% Triton-X in PBS. For biotin detection, either an anti-biotin antibody (1:1000, ImmuneChen, ICP0611) or Alexa647-conjugated streptavidin (1:1000, ApexBio, K4406) were used. The primary antibody, secondary antibody (1:1000, Jackson ImmunoResearch, 711-605-152), and fluorescence-labeled streptavidin were diluted in Antibody Buffer containing 0.5% BSA, 5% normal donkey serum and 0.25% Triton-X in PBS.

To fluorescently label the alkyne group, the Click-iT Imaging Kit (Thermo Fisher, C10340) was used according to the manufacturer's instructions. The cells were counterstained with DAPI (1 μg $ml^{-1}$) and imaged using a Zeiss LSM 980 confocal microscope.

Flow cytometry was used to assess the expression of H2B-BmTyr-mCherry and the cytotoxic effect of $Cu^{2+}$ incubation on T cells. The cells were washed twice with ice-cold PBS and then resuspended in FACS Buffer (1% FBS, 0.25% BSA in PBS). Additionally, the cells were counterstained with DAPI to differentiate between live and dead cells.

### 4.9. CuAAC click reaction for cell lysate

The cells were washed twice with PBS and then centrifuged at 500×*g* for 5 min. Subsequently, the cells were lysed with lysis buffer composed of PBS, 0.1% Igepal CA-630 (Sigma, 9002-93-1), and protease inhibitor cocktail (MCE, HY-K0010) for 30 min. Following sonication on ice, the cell lysates were centrifuged at 12,000 rpm for 15 min at 4 °C. The protein concentration was determined using BCA Protein Assay Kit according to the manufacturer's instructions (NCM, WB6501) and was normalized to 2 mg $ml^{-1}$.

For the CuAAC click reaction for mass spectrometry analysis, the Cu/BTTAA/TCEP kit (Chomixbiotech, 02030008) was used to conjugate alkyne-labeled proteins to azide magnetic beads (Chomixbiotech, 02030004). In brief, azide magnetic beads were washed three times with

PBS and resuspended with 100 μl of protein lysate. Subsequently, 5.5 μl of BTTAA/CuSO4 (25 × ) and 2.7 μl of TCEP (50 × ) were added and mixed well. The sample was reacted for 3 h at room temperature using a thermomixer. Following the click reaction, the beads were washed three times with PBS containing 0.2% SDS, and then washed an additional three times with PBS before being snap-frozen in liquid nitrogen for mass-based analysis.

For CuAAC click reaction for immunoprecipitation and Western blotting detection, the Cu/BTTAA kit (Chomixbiotech, #02030001) was used to conjugate alkyne-labeled proteins to azide-tagged peptides. In brief, 0.5 μl of 5 mM Fmoc-Lys (N3)-conjugated HiBiT tag (custom made, KS-V peptide, MW 1763.01), 0.5 μl of 5 mM 10 × His azide (AAT Bioquest, 12642, MW 1641.71), 2 μl of BTTAA/CuSO4 mixture (25 × ), and 2 μl of Na-Ascorbate solution (25 × ) were added to the 50 μl of the protein lysate and mixed well. The sample was then reacted for 1 h at room temperature using a thermomixer.

### 4.10. LC-MS/MS analysis

For liquid Chromatography with tandem mass spectrometry (LC-MS-MS) analysis, the beads were resuspended in 100 μl of lysis buffer containing 5 mM dithiothreitol and reduced at 56 °C for 30 min. For global proteomics, cells were sonicated three times on ice in lysis buffer (8 M urea, 1% protease inhibitor cocktail), and centrifuged at 12,000 rpm for 15 min at 4 °C.The supernatant was collected, and the protein concentration was determined using BCA Protein Assay Kit according to the manufacturer's instructions. An equal amount of protein from each sample was taken and adjusted to the same volume with lysis buffer containing 5 mM dithiothreitol and reduced at 56 °C for 30 min. The protein was subsequently alkylated with 11 mM iodoacetamide for 15 min at room temperature in the dark. The solution was then diluted with 200 mM TEAB to ensure that the concentration of urea remained below 2 M. Trypsin was added at a ratio of 1:50 and incubated overnight for enzymatic hydrolysis. Finally, the peptides were desalted using a Strata X SPE column. The tryptic peptides were dissolved in solvent A, and directly loaded onto a home-made reversed-phase analytical column (15 cm length, 100 μm i.d.) using a Vanquish Neo UPLC system (Thermo Fisher) at a flow rate of 600 nl $min^{-1}$. The mobile phase consisted of solvent A (0.1% formic acid in water) and Solvent B (0.1% formic acid in 80% acetonitrile). The following gradient was applied: 4% Solvent B (0−0.5 min); 4%-7.5% Solvent B (0.5−0.6 min); 7.5%-30% Solvent B (0.6−8.1 min); 30%-44% Solvent B (8.1−9.6 min); 44%-55% Solvent B (9.6−10 min); 55%-99% Solvent B (10−10.5 min); 99% Solvent B (10.5−12 min). The eluted peptides were analyzed on a timsTOF HT mass spectrometer via a capillary ion source in data independent parallel accumulation serial fragmentation (dia-PASEF) mode. An electrospray voltage of 1.6 kV was applied. The full MS scan ranges were *m/z* 300-1500, and 12 PASEF MS/MS scans were acquired per cycle. The MS/MS scan range was set as 395−1080 with an isolation window of 15 m $z^{-1}$.

Raw DIA (Data-Independent Acquisition) data were processed using DIA-NN (v.1.8). The tandem mass spectra were searched against the *Mus musculus* UniProt reference proteome (UP000000589, 10090_SP_20241202.fasta, containing 17,236 entries or 10090 SP 20251219.fasta, containing 17247 entries, respectively), concatenated with a reverse decoy database. Trypsin/P was specified as the digestion enzyme, allowing up to one missed cleavage. Fixed modifications included the excision of N-terminal Methionine and carbamidomethyl Cysteine. The false discovery rate (FDR) was adjusted to be less than 1%.

For each protein, the normalized intensity (*NI*) was derived from the DIA-NN output. To enable cross-sample comparison, the relative normalized intensity (*RI*) was calculated as:

$RI_{ij} = NI_{ij}/\text{mean}\ (NI_j)$, where *i* denotes the sample and *j* denotes the protein. This value was used to quantitatively compare protein abundance across experimental conditions. Proteins with a fold change >1.5 were considered enriched, and proteins with a fold change <1/1.5 (i.e., <0.67) were considered decreased.

The eggNOG-mapper (v2.1.6) was used to identify proteins based on the EggNOG database (v5.0.2, http://eggnog5.embl.de/#/app/home) followed by Gene Ontology (GO) functional annotation analysis on the proteins according to cellular components, molecular functions, and biological processes. The full MS hit quantification and GO biological process data are provided in Supplement File 2 and Supplement File 3.

### 4.11. Immunoprecipitation

Following the CuAAC reaction, the protein lysate mixture was dialyzed overnight at 4 °C using a Slide-A-Lyzer MINI Dialysis Unit (Thermo Fisher, 69574) to remove unconjugated peptides. The proteins were recovered, and the volume was adjusted to 100 μl with Binding Buffer (PBS, 10 mM Imidazole, pH 7.4). Subsequently, 10 μl of the protein sample were collected as input sample. To purify the click reaction-labeled proteins, 25 μl of Ni-NTA beads (Yeasen, 20561ES03) were washed three times with Binding Buffer and then resuspended in the remaining 90 μl of the protein sample, followed by overnight incubation at 4 °C. The beads were washed three times with Washing Buffer (PBS, 20 mM Imidazole, pH 7.4) and eluted with 50 μl of Elution Buffer (PBS, 350 mM Imidazole, pH 7.4) at room temperature for 5 min.

To evaluate the elution efficiency of streptavidin beads, the dialysis samples were recovered, and the volume was adjusted to 100 μl with PBST. An aliquot of 10 μl of the protein sample was collected as the input sample, while the remaining 90 μl was incubated overnight at 4 °C with 25 μl of pre-equilibrated streptavidin beads (AlpaLifeBio, KTSM1348). The beads were washed three times with PBST and subsequently eluted with 50 μl of 25 mM biotin at 95 °C for 5 min or 95% formamide containing 10 mM EDTA (pH 8.2) at 95 °C for 5 min. The eluted proteins were mixed with 5 × SDS-PAGE loading buffer (NCM, WB2001) and denatured at 95 °C for 5 min. The post-elution beads were boiled in 1 × SDS-PAGE loading buffer at 95 °C for 5 min.

### 4.12. Nuclear protein extraction

Nuclear proteins were extracted using the Nuclear and Cytoplasmic Protein Extraction Kit (Beyotime, #P0027). Briefly, the cells were washed with PBS and centrifuged at 500×*g* for 5 min. The cell pellet was then resuspended in 200 μl of Cytoplasmic Protein Extraction Reagent A, supplemented with protease inhibitor cocktail (MCE, HY-K0010). The suspension was vortexed vigorously and incubated on ice for 15 min. Subsequently, 10 μl of Cytoplasmic Protein Extraction Reagent B was added, and the mixture was centrifuged at 12000 rpm for 5 min at 4 °C. The resulting supernatant contained the cytoplasmic proteins, while the pellet was resuspended in 50 μl of Nuclear Protein Extraction Reagent, also containing a protease inhibitor cocktail. This sample was vortexed vigorously for 30 s and incubated on ice for 30 min. Following this, the sample was centrifuged at 12,000 rpm for 15 min at 4 °C. The proteins were denatured at 95 °C for 5 min in 5 × SDS-PAGE loading buffer. Finally, the proteins were separated by SDS-PAGE and immunoblotted with the indicated antibodies.

### 4.13. Western blotting

The lysates were subsequently mixed with 5 × SDS-PAGE loading buffer (NCM, WB2001) and denatured at 95 °C for 5 min. Proteins were then separated using SDS-PAGE and transferred to nitrocellulose membranes for HiBiT tag detection, or to PVDF membranes for the detection of other proteins. Membranes were stained with Ponceau S solution (KeyGEN, KGB4305-120) for 10 min and washed with deionized water until the background was clear. Membranes were then imaged.

For HiBiT tag detection, nitrocellulose membranes were incubated in TBST for 1 h at room temperature and then transferred to Nano-Glo blotting buffer (Promega, N2410, diluted 1:10) to facilitate the binding of LgBiT Protein (diluted 1:200) to HiBiT tag-conjugated proteins on

the membrane at 4 °C overnight. Following this, Nano-Glo® Luciferase Assay Substrate (Promega, N2410, diluted 1:500) was added and incubated at room temperature for 5 min.

For the detection of other proteins, the PVDF membranes were blocked with 5% skim milk powder in TBST at room temperature for 2 h and subsequently incubated with primary antibodies at 4 °C overnight. Following three washes with TBST, the membranes were incubated with HRP-conjugated secondary antibodies at room temperature for 1 h. The membranes were then washed three times with TBST. Imaging was performed using the NcmECL Ultra Chemiluminescent Kit (NCM, P10100). The following primary antibodies were used: rabbit anti-NKAP (Jotbody, JOT-AP11886, 1:2000), rabbit anti-LaminB1 (Proteintech, 12987-1-AP, 1:10000), rabbit anti-GAPDH (NCM, #AB2020, 1:5000), rabbit anti-biotin (ImmuneChem, #ICP0611, 1:4000) and rabbit anti-mCherry (Abcam, #ab167453, 1:1000). The secondary antibody used was goat anti-rabbit IgG-HRP (Abcam, #ab205718, 1:10000). Protein detection on the membranes were performed using a chemiluminescence imaging system (Tanon-5200).

### 4.14. Statistics

Immunofluorescence images and blotting images were analyzed in FIJI. Graphics and statistical analyses were performed using Prism V9. Experiments were repeated three times independently. The *P* values were determined based on biological replicates.

## CRediT authorship contribution statement

**Xin-Nan Zheng:** Conceptualization, Data curation, Formal analysis, Writing – original draft, Writing – review & editing. **Jing-Min Zeng:** Data curation. **Han-Ying Huang:** Data curation, Writing – original draft. **Chuang Zhao:** Formal analysis. **Sheng-Suo Ma:** Methodology. **Lin Feng:** Methodology. **Hao Zhu:** Conceptualization, Methodology. **Lin Tian:** Conceptualization, Data curation, Formal analysis, Funding acquisition, Investigation, Methodology, Project administration, Resources, Supervision, Validation, Visualization, Writing – original draft, Writing – review & editing.

## Declaration of competing interest

The Authors declare no Competing Financial or Non-Financial Interests.

## Acknowledgment

LT is supported by the National Natural Science Foundation (NSFC) of China (Grant No. 82573221) and Young Talents Program of SYSUCC (Grant No. YTP-SYSUCC-0045).

## Appendix A. Supplementary data

Supplementary data to this article can be found online at https://doi.org/10.1016/j.bbrc.2026.153918.

## References

[1] D. Eisenberg, E.M. Marcotte, I. Xenarios, T.O. Yeates, Protein function in the post-genomic era, Nature 405 (2000) 823–826, https://doi.org/10.1038/35015694.
[2] G. Millan-Zambrano, A. Burton, A.J. Bannister, R. Schneider, Histone post-translational modifications - cause and consequence of genome function, Nat. Rev. Genet. 23 (2022) 563–580, https://doi.org/10.1038/s41576-022-00468-7.
[3] M.Y. Hein, N.C. Hubner, I. Poser, J. Cox, N. Nagaraj, Y. Toyoda, I.A. Gak, I. Weisswange, J. Mansfeld, F. Buchholz, et al., A human interactome in three quantitative dimensions organized by stoichiometries and abundances, Cell 163 (2015) 712–723, https://doi.org/10.1016/j.cell.2015.09.053.
[4] E.L. Huttlin, L. Ting, R.J. Bruckner, F. Gebreab, M.P. Gygi, J. Szpyt, S. Tam, G. Zarraga, G. Colby, K. Baltier, et al., The BioPlex network: a systematic exploration of the human interactome, Cell 162 (2015) 425–440, https://doi.org/10.1016/j.cell.2015.06.043.
[5] A. Paiano, A. Margiotta, M. De Luca, C. Bucci, Yeast two-hybrid assay to identify interacting proteins, Curr. Protoc. Protein Sci. 95 (2019) e70, https://doi.org/10.1002/cpps.70.
[6] S.M. Gustafsdottir, E. Schallmeiner, S. Fredriksson, M. Gullberg, O. Soderberg, M. Jarvius, J. Jarvius, M. Howell, U. Landegren, Proximity ligation assays for sensitive and specific protein analyses, Anal. Biochem. 345 (2005) 2–9, https://doi.org/10.1016/j.ab.2005.01.018.
[7] A. Brymora, V.A. Valova, P.J. Robinson, Protein-protein interactions identified by pull-down experiments and mass spectrometry, Curr. Protoc. Cell Biol. Chapter 17 (2004), https://doi.org/10.1002/0471143030.cb1705s22. Unit 17 15.
[8] J.F. Greenblatt, B.M. Alberts, N.J. Krogan, Discovery and significance of protein-protein interactions in health and disease, Cell 187 (2024) 6501–6517, https://doi.org/10.1016/j.cell.2024.10.038.
[9] B. Turriziani, A. Garcia-Munoz, R. Pilkington, C. Raso, W. Kolch, A. von Kriegsheim, On-beads digestion in conjunction with data-dependent mass spectrometry: a shortcut to quantitative and dynamic interaction proteomics, Biology 3 (2014) 320–332, https://doi.org/10.3390/biology3020320.
[10] J. Noone, R.G. Wallace, K.D. Rochfort, Immunoprecipitation: variations, considerations, and applications, Methods Mol. Biol. 2699 (2023) 271–303, https://doi.org/10.1007/978-1-0716-3362-5_15.
[11] J.E. Cronan, Biotin protein ligase as you like it: either extraordinarily specific or promiscuous protein biotinylation, Proteins 92 (2024) 435–448, https://doi.org/10.1002/prot.26642.
[12] B.S. Johnson, L. Chafin, D. Farkas, J. Adair, A. Elhance, L. Farkas, J.S. Bednash, J. D. Londino, MicroID2: a novel biotin ligase enables rapid proximity-dependent proteomics, Mol. Cell. Proteomics 21 (2022) 100256, https://doi.org/10.1016/j.mcpro.2022.100256.
[13] T.C. Branon, J.A. Bosch, A.D. Sanchez, N.D. Udeshi, T. Svinkina, S.A. Carr, J. L. Feldman, N. Perrimon, A.Y. Ting, Efficient proximity labeling in living cells and organisms with TurboID, Nat. Biotechnol. 36 (2018) 880–887, https://doi.org/10.1038/nbt.4201.
[14] L. Kubitz, S. Bitsch, X. Zhao, K. Schmitt, L. Deweid, A. Roehrig, E.C. Barazzone, O. Valerius, H. Kolmar, J. Bethune, Engineering of ultraID, a compact and hyperactive enzyme for proximity-dependent biotinylation in living cells, Commun. Biol. 5 (2022) 657, https://doi.org/10.1038/s42003-022-03604-5.
[15] Z.B. Hill, S.B. Pollock, M. Zhuang, J.A. Wells, Direct proximity tagging of small molecule protein targets using an engineered NEDD8 ligase, J. Am. Chem. Soc. 138 (2016) 13123–13126, https://doi.org/10.1021/jacs.6b06828.
[16] Q. Liu, J. Zheng, W. Sun, Y. Huo, L. Zhang, P. Hao, H. Wang, M. Zhuang, A proximity-tagging system to identify membrane protein-protein interactions, Nat. Methods 15 (2018) 715–722, https://doi.org/10.1038/s41592-018-0100-5.
[17] S.S. Lam, J.D. Martell, K.J. Kamer, T.J. Deerinck, M.H. Ellisman, V.K. Mootha, A. Y. Ting, Directed evolution of APEX2 for electron microscopy and proximity labeling, Nat. Methods 12 (2015) 51–54, https://doi.org/10.1038/nmeth.3179.
[18] E. Choi-Rhee, H. Schulman, J.E. Cronan, Promiscuous protein biotinylation by Escherichia coli biotin protein ligase, Protein Sci. 13 (2004) 3043–3050, https://doi.org/10.1110/ps.04911804.
[19] K.F. Cho, T.C. Branon, S. Rajeev, T. Svinkina, N.D. Udeshi, T. Thoudam, C. Kwak, H.W. Rhee, I.K. Lee, S.A. Carr, A.Y. Ting, Split-TurboID enables contact-dependent proximity labeling in cells, Proc. Natl. Acad. Sci. U. S. A. 117 (2020) 12143–12154, https://doi.org/10.1073/pnas.1919528117.
[20] S.Y. Lee, J.S. Cheah, B. Zhao, C. Xu, H. Roh, C.K. Kim, K.F. Cho, N.D. Udeshi, S. A. Carr, A.Y. Ting, Engineered allostery in light-regulated LOV-turbo enables precise spatiotemporal control of proximity labeling in living cells, Nat. Methods 20 (2023) 908–917, https://doi.org/10.1038/s41592-023-01880-5.
[21] W. Qin, J.S. Cheah, C. Xu, J. Messing, B.D. Freibaum, S. Boeynaems, J.P. Taylor, N. D. Udeshi, S.A. Carr, A.Y. Ting, Dynamic mapping of proteome trafficking within and between living cells by TransitID, Cell 186 (2023) 3307–3324.e3330, https://doi.org/10.1016/j.cell.2023.05.044.
[22] H.W. Rhee, P. Zou, N.D. Udeshi, J.D. Martell, V.K. Mootha, S.A. Carr, A.Y. Ting, Proteomic mapping of mitochondria in living cells via spatially restricted enzymatic tagging, Science 339 (2013) 1328–1331, https://doi.org/10.1126/science.1230593.
[23] J.C. Maza, D.L.V. Bader, L. Xiao, A.M. Marmelstein, D.D. Brauer, A.M. ElSohly, M. J. Smith, S.W. Krska, C.A. Parish, M.B. Francis, Enzymatic modification of N-Terminal proline residues using phenol derivatives, J. Am. Chem. Soc. 141 (2019) 3885–3892, https://doi.org/10.1021/jacs.8b10845.
[24] J.D. Martell, T.J. Deerinck, Y. Sancak, T.L. Poulos, V.K. Mootha, G.E. Sosinsky, M. H. Ellisman, A.Y. Ting, Engineered ascorbate peroxidase as a genetically encoded reporter for electron microscopy, Nat. Biotechnol. 30 (2012) 1143–1148, https://doi.org/10.1038/nbt.2375.
[25] Y. Che, P.A. Khavari, Research techniques made simple: emerging methods to elucidate protein interactions through spatial proximity, J. Invest. Dermatol. 137 (2017) e197–e203, https://doi.org/10.1016/j.jid.2017.09.028.
[26] H. Zhu, J.H. Oh, Y. Matsuda, T. Mino, M. Ishikawa, H. Nakamura, M. Tsujikawa, H. Nonaka, I. Hamachi, Tyrosinase-based proximity labeling in living cells and in vivo, J. Am. Chem. Soc. 146 (2024) 7515–7523, https://doi.org/10.1021/jacs.3c13183.
[27] Z. Zhang, Y. Wang, W. Lu, X. Wang, H. Guo, X. Pan, Z. Liu, Z. Wu, W. Qin, Spatiotemporally resolved mapping of extracellular proteomes via in vivo-compatible TyroID, Nat. Commun. 16 (2025) 2553, https://doi.org/10.1038/s41467-025-57767-w.
[28] Y. Li, C. Tian, K. Liu, Y. Zhou, J. Yang, P. Zou, A clickable APEX probe for proximity-dependent proteomic profiling in yeast, Cell Chem. Biol. 27 (2020) 858–865 e858, https://doi.org/10.1016/j.chembiol.2020.05.006.

[29] K.P. van Gisbergen, N.A. Kragten, K.M. Hertoghs, F.M. Wensveen, S. Jonjic, J. Hamann, M.A. Nolte, R.A. van Lier, Mouse hobit is a homolog of the transcriptional repressor Blimp-1 that regulates NKT cell effector differentiation, Nat. Immunol. 13 (2012) 864–871, https://doi.org/10.1038/ni.2393.
[30] L.K. Mackay, M. Minnich, N.A. Kragten, Y. Liao, B. Nota, C. Seillet, A. Zaid, K. Man, S. Preston, D. Freestone, et al., Hobit and Blimp1 instruct a universal transcriptional program of tissue residency in lymphocytes, Science 352 (2016) 459–463, https://doi.org/10.1126/science.aad2035.
[31] J.S. Cheah, S. Yamada, A simple elution strategy for biotinylated proteins bound to streptavidin conjugated beads using excess biotin and heat, Biochem. Biophys. Res. Commun. 493 (2017) 1522–1527, https://doi.org/10.1016/j.bbrc.2017.09.168.
[32] Y.L. Liu, Z.Y. Guo, The NanoBiT-Based homogenous ligand-receptor binding assay, Methods Mol. Biol. 2525 (2022) 139–153, https://doi.org/10.1007/978-1-0716-2473-9_10.
[33] C. Ascanelli, E. Lawrence, C.A.P. Batho, C.H. Wilson, A flexible, high-throughput system for studying live mRNA translation with HiBiT technology, Nucleic Acids Res. 53 (2025), https://doi.org/10.1093/nar/gkaf496.
[34] D.C. Ranawakage, T. Takada, Y. Kamachi, HiBiT-qIP, HiBiT-based quantitative immunoprecipitation, facilitates the determination of antibody affinity under immunoprecipitation conditions, Sci. Rep. 9 (2019) 6895, https://doi.org/10.1038/s41598-019-43319-y.
[35] J.S. Kim, C.A. Valencia, R. Liu, W. Lin, Highly-efficient purification of native polyhistidine-tagged proteins by multivalent NTA-Modified magnetic nanoparticles, Bioconjug. Chem. 18 (2007) 333–341, https://doi.org/10.1021/bc060195l.
[36] S. Willems, V. Morozov, J.A. Marschner, D. Merk, Comparative profiling and chemogenomics application of chemical tools for NR4A nuclear receptors, J. Med. Chem. 68 (2025) 19955–19970, https://doi.org/10.1021/acs.jmedchem.5c00459.
[37] H. Cheng, S. Li, H. Liu, M. Yan, J. Wang, J. Huang, S. Liu, Y. Yang, X. Cao, P. Cui, et al., Mycobacterium tuberculosis-derived linoleic acid increases regulatory T cell function to promote bacterial survival within macrophages, Nat. Microbiol. 10 (2025) 2949–2965, https://doi.org/10.1038/s41564-025-02140-2.
[38] J. An, C.P. Zhang, H.Y. Qiu, H.X. Zhang, Q.B. Chen, Y.M. Zhang, X.L. Lei, C. X. Zhang, H. Yin, Y. Zhang, Enhancement of the viability of T cells electroporated with DNA via osmotic dampening of the DNA-sensing cGAS-STING pathway, Nat. Biomed. Eng. 8 (2024) 149–164, https://doi.org/10.1038/s41551-023-01073-7.
[39] M.S. Hayden, S. Ghosh, Regulation of NF-kappaB by TNF family cytokines, Semin. Immunol. 26 (2014) 253–266, https://doi.org/10.1016/j.smim.2014.05.004.
[40] S. Blanchett, I. Boal-Carvalho, S. Layzell, B. Seddon, NF-kappaB and extrinsic cell death pathways - entwined do-or-die decisions for T cells, Trends Immunol. 42 (2021) 76–88, https://doi.org/10.1016/j.it.2020.10.013.
[41] A. Israel, The IKK complex, a central regulator of NF-kappaB activation, Cold Spring Harbor Perspect. Biol. 2 (2010) a000158, https://doi.org/10.1101/cshperspect.a000158.
[42] R.E. Lee, S.R. Walker, K. Savery, D.A. Frank, S. Gaudet, Fold change of nuclear NF-kappaB determines TNF-induced transcription in single cells, Mol. Cell 53 (2014) 867–879, https://doi.org/10.1016/j.molcel.2014.01.026.
[43] D. Chen, Z. Li, Q. Yang, J. Zhang, Z. Zhai, H.B. Shu, Identification of a nuclear protein that promotes NF-kappaB activation, Biochem. Biophys. Res. Commun. 310 (2003) 720–724, https://doi.org/10.1016/j.bbrc.2003.09.074.
[44] X. Zhang, J. Duan, Y. Li, X. Jin, C. Wu, X. Yang, W. Lu, W. Ge, NKAP acts with HDAC3 to prevent R-loop associated genome instability, Cell Death Differ. 30 (2023) 1811–1828, https://doi.org/10.1038/s41418-023-01182-5.
[45] M.J. Shapiro, M.J. Lehrke, J.Y. Chung, S. Romero Arocha, V.S. Shapiro, NKAP must associate with HDAC3 to regulate hematopoietic stem cell maintenance and survival, J. Immunol. 202 (2019) 2287–2295, https://doi.org/10.4049/jimmunol.1800862.
[46] Y. Yang, J. Wu, L. Wang, G. Ji, Y. Dang, Copper homeostasis and cuproptosis in health and disease, MedComm (2024) 5–e724, https://doi.org/10.1002/mco2.724, 2020.
[47] H. Zhu, T. Tamura, A. Fujisawa, Y. Nishikawa, R. Cheng, M. Takato, I. Hamachi, Imaging and profiling of proteins under oxidative conditions in cells and tissues by hydrogen-peroxide-responsive labeling, J. Am. Chem. Soc. 142 (2020) 15711–15721, https://doi.org/10.1021/jacs.0c02547.
[48] S. Zhang, Q. Tang, X. Zhang, X. Chen, Proximitomics by reactive species, ACS Cent. Sci. 10 (2024) 1135–1147, https://doi.org/10.1021/acscentsci.4c00373.
[49] J. Paek, M. Kalocsay, D.P. Staus, L. Wingler, R. Pascolutti, J.A. Paulo, S.P. Gygi, A. C. Kruse, Multidimensional tracking of GPCR signaling via peroxidase-catalyzed proximity labeling, Cell 169 (2017) 338–349.e311, https://doi.org/10.1016/j.cell.2017.03.028.
[50] S.D. Knutson, B.F. Buksh, S.W. Huth, D.C. Morgan, D.W.C. MacMillan, Current advances in photocatalytic proximity labeling, Cell Chem. Biol. 31 (2024) 1145–1161, https://doi.org/10.1016/j.chembiol.2024.03.012.
[51] S. Gluck, B. Guey, M.F. Gulen, K. Wolter, T.W. Kang, N.A. Schmacke, A. Bridgeman, J. Rehwinkel, L. Zender, A. Ablasser, Innate immune sensing of cytosolic chromatin fragments through cGAS promotes senescence, Nat. Cell Biol. 19 (2017) 1061–1070, https://doi.org/10.1038/ncb3586.
[52] Q. Chen, L. Sun, Z.J. Chen, Regulation and function of the cGAS-STING pathway of cytosolic DNA sensing, Nat. Immunol. 17 (2016) 1142–1149, https://doi.org/10.1038/ni.3558.